Journal of Materials Chemistry C

Accepted Manuscript

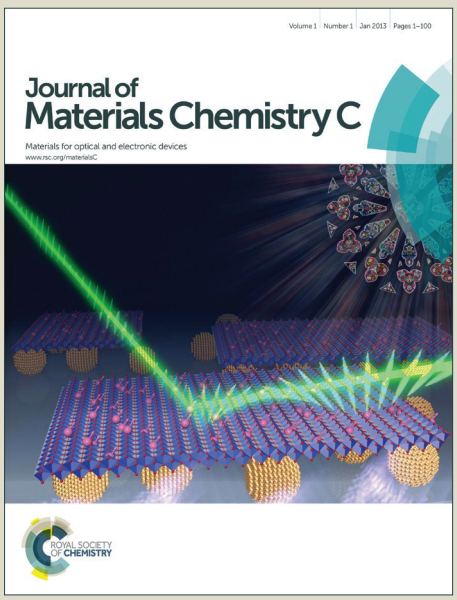

ROYAL SOCIETY OF CHEMISTRY

www.rsc.org/materialsC

Influence of PbS layer on optical and electronic properties of ZnO@PbS core-shell nanorods thin film

Mrinmoy Misra, Suman Singh, A. K. Paul, Madan Lal Singla

Academy of Scientific & Innovative Research (AcSIR), Council for Scientific and Industrial Research (CSIR), Central Scientific Instruments Organisation (CSIO), Material Research Division, Sector 30 C, Chandigarh, India
Email ID: mrinmoymishra@gmail.com
Phone Number: +91-9803473089
Fax: +91-172-2657267

Abstract:

In present work, ZnO@PbS core-shell thin film based solar cell has been fabricated using successive ionic layer absorption and reaction method (SILAR). The assembly consists of zinc oxide (ZnO) nanorods as core and PbS as shell and the thickness of PbS layer was controlled by varying the number of dipping cycles. The varied PbS layer thickness resulted in the shifting of the absorption of ZnO@PbS from ultraviolet region to the visible region. The PbS layer supressed the visible emission of ZnO and enhanced the charge separation at the interface. By introducing PbS layers the charge generation and separation within the ZnO@PbS core-shell nanorod has been improved. The PbS shell on ZnO nanorods improved the short-circuit current (J_{sc}), open circuit voltage (V_{oc}) and fill factor (FF), which in-turn resulted in the enhancement of photovoltaic device efficiency. The maximum power conversion efficiency of 6.59 % was achieved with ten layers of PbS in ZnO@PbS@Dye thin film based solar cell.

1.0 Introduction:

Now-a-days semiconductor nanostructures are drawing attention of the researchers for the development of dye-sensitized solar cells (DSSc) because of their superior optoelectronic properties at nanoscale region [1, 2]. The band gap and absorption range can be tuned by adjusting the size and shape of the nanostructure material due to quantum confinement [3]. The one-dimensional (1D) nanorods of metal oxide like tin dioxide (TiO_2) and zinc oxide (ZnO) have been considered as synthetically tunable nanoscale building blocks for next-generation electronic devices. These materials have some properties such as: quantum confinement effects in the radial axis, large aspect ratio, high directional electron mobility, more electron diffusion length, less charge recombination rate and good electron-acceptor [4, 5]. These properties make them very useful material for being used as electrodes, in energy conversion and storage devices. ZnO nanorods have higher electron mobility (~205-1000 $cm^2\ V^{-1}\ s^{-1}$) than TiO_2 (~0.1-4 $cm^2\ V^{-1}\ s^{-1}$) and can perform fast diffusion transport of photo injected electrons when used as anode in DSSc [6]. But still the ZnO nanorods have failed to draw the attention of the researchers.

It is expected that PbS nanostructure can further improve the photo catalytic activity of ZnO due to efficient spatial separation of photo generated electron, and can also prevent electron-hole recombination at the interface of two materials. The PbS nanostructure are very advantageous due to their specific properties such as narrow band gap (0.41 eV), for bulk, excellent photosensitivity in the near-IR, large excitonic Bohr radius (□18 nm), high dielectric constants and small effective mass for electron and hole [7, 8]. In recent years, a lot of work on CdS, CdSe and PbSe nanoparticle or quantum dot sensitized solar cells with high photoconversion efficiency has been reported [9-13]. Various studies have been reported on the development of the methods for synthesis of the tunable size PbS nanocrystal to absorb the light on the near- NIR region [14, 15]. PbS layer can be deposited on the surface of metal oxides by chemical bath deposition (CBD) or by successive ionic layer adsorption/reaction (SILAR) or pre-synthesized nanostructure soaking method.

The core-shell nanostructures on other hand, have their own advantages like ability to enhance the efficiency of the interfacial charge separation process and to achieve Fermi level equilibrium. Moreover, these structures have a controllable chemical composition and

chemical stability, and are able to electrically insulate the core material from its surroundings[16].

Recently, many synthesis routes have been developed to synthesize ZnO@PbS core-shell nanostructure. Among the reported methods, Wang and co-workers spin-coated the PbS quantum dot on ZnO nanowire (NW) arrays and studied the effect of ZnO NW dimensions and density to achieve higher efficiency in the near-IR region [17]. GaO and co-workers prepared ZnO/PbS quantum dot (QD) based thin film and studied the effect of size on overall performance of solar cells. They also reported that the Schottky barrier height is a function of the quantum dot band gap energy and back contact metal work function [18]. Brown and co-workers prepared ZnO/PbS heterojunction QD based solar cell where MoO_3 interlayer was used between the PbS QDs and anode electrode. The power conversion efficiency was about 3.5 ± 0.4 % for a device employing a gold anode [19]. Will and co-workers prepared ZnO/PbS QDs based solar cell and studied the charge separation at the heterojunction interface of ZnO/PbS. Further, they investigated the impedance and external quantum efficiency response to examine the effect of zinc oxide doping density [20]. Jean and co-works prepared a ZnO/PbS ordered QDs solar cell and studied the effect of thickness of the MoO_3 anode layer. The maximum energy conversion efficiency and fill factor achieved was 4.3 % and 0.4 respectively [21]. Song and co-worker prepared ZnO@PbS core-shell nanorod array based thin film and used it as a counter electrode for quantum dot sensitized solar cells. The maximum fill factor and efficiency of fabricated solar cell was 0.52 and 3.05 % respectively [22]. So far, many researchers worked on preparation of TiO_2 and TiO_2/PbS nanostructure for solar cell and many other applications [23-31]. A study has shown that the life time of excitons in ZnO@CdS nanorods can be enhanced by varying the thickness of CdS coating[32].

To the best of our knowledge, this promising ZnO@PbS core-shell electrode with variable PbS shell layers have not been employed in dye-sensitized solar cells so far. We studied the effect of PbS shell layer thickness on the life time of excitons. Particular attention was focused on the control of the PbS layer thickness on ZnO nanorods to achieve higher efficiency in the solar cell. We demonstrated that the increasing PbS shell thickness led to the enhancement in the short-circuit current (J_{sc}), open-circuit voltage (V_{oc}) and fill factor (FF) of the device. The maximum power conversion efficiency and fill factor was 6.59 % and 0.75 respectively.

2. Experimental

2.1 Preparation of ZnO seed layers

Prior to the deposition of ZnO seed on four indium tin oxide (ITO) glass substrates, they were ultrasonically cleaned for 40 min in a mixture of acetone, isopropyl alcohol and deionised water. Zinc acetate (0.1 M) solution was prepared in 50 mL of methanol and heated at about 45 °C in a covered glass beaker with continuous stirring for 20 minutes. Then 50 mL of sodium hydroxide (0.4 M) in methanol was added to form a transparent solution. The temperature of the mixture was maintained at 45 °C. ITO substrates were dipped in the reaction bath and the solution was stirred continuously for 2 h. After deposition, each ZnO seed coated samples were annealed at 200 °C for 1 h to remove residual organics. The seed layer coated ITO substrates were further used for the growth of ZnO nanorods.

2.2 Growth of ZnO nanorods (ZNR)

The four ZnO seed layer coated ITO substrates were immersed in a mixture of aqueous solution containing 100 mL of zinc nitrate (50 mM) and 100 mL of hexamethylenetetramine (HMT) (50 mM). The mixture was then heated on a hot plate at 95 °C temperature for 1 h with continuous stirring. Each thin film was thoroughly rinsed with deionized water to remove impurity and dried in atmosphere at 200°C for 3 h. The prepared ZnO nanorods thin films samples were named as S1, S2, S3 and S4.

2.3 Synthesis of ZnO@PbS core-shell thin film using SILAR method:

Previously prepared ZnO nanorods (ZNR) electrodes (sample S2, S3 and S4) were dipped in 1% mercaptopropionic acid (MPA) solution for 1 minute and were dried at 80 °C for 3 hours. The mercaptopropionic acid caped ZnO nanorods were coated with PbS by the successive ionic layer absorption and reaction (SILAR) method. The ZNR electrodes were exposed to Pb^{2+} and S^{2-} ions by successive immersion in an aqueous solution of 0.01 M lead nitrate and an aqueous solution of 0.01 M sodium sulfide. The electrodes were washed with ethanol and DI water in the intermediate steps. The number of cycles of PbS layer were 3, 5 and 10 for

sample S2, S3 and S4 respectively. Upon completion of each cycle, a thin layer of PbS layer was deposited onto the ZNR surface, as shown in equation 1.

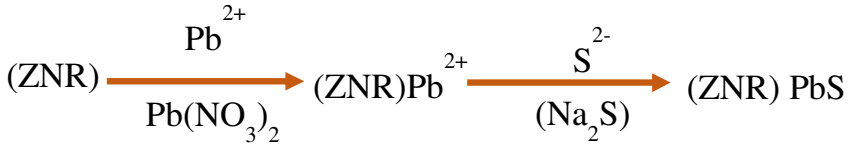

(1)

2.4 Dye-Sensitized ZnO/ZnO@PbS thin film preparation and Cell Fabrication:

For dye-sensitized ZnO/ZnO@PbS thin film preparation the electrodes (sample S1 to S4) were soaked in an aqueous solution of ruthenium dye (3 mM, N719) at room temperature for 24 h. The prepared thin films were named as a $S1^{*}$, $S2^{*}$, $S3^{*}$ and $S4^{*}$. A platinum (Pt) layer coated ITO substrate was used as counter electrode. In fabricating the cell, the two electrodes were held together with clips, and separated by a Teflon spacer having a thickness of 40 μm. The electrolyte solution consisting of 1 M Na_2S and 1 M S in aqueous solution was introduced into the thin film by capillary draw action.

3. Characterization methods:

The UV– Vis spectra were recorded on a Hitachi U-3900H spectrophotometer coupled with a 1.00 cm quartz cell. The potoluminescence (PL) spectra and life time decay were performed on Cary Eclipse Fluorescence spectrometer under the excitation of 350 nm. X-ray diffraction (XRD) patterns were taken on a Philip-X'Pert X-ray diffractometer with a Cu Kα X-ray source. The morphology of ZnO nanorods and PbS nanostructures was recorded on Field emission scanning electron microscope (FE-SEM) (Hitachi 4300 SE/N) and Transmission Electron Microscope (TEM) (JEM-200 CX). For TEM studies, the thin films were scratched and sonicated in aqueous solution. The photocurrent-voltage characteristics were measured with a Keithley 2400 source meter under illumination from a 150 W xenon lamp. The FTIR of ZnO nanorod and ZnO@PbS thin film were studied on Varian FTIR system (600 series). For sample preparation, the thin film were scratched and mixed with KBr for palate preparation. The amperometric measurements was performed with a CHI 680

electrochemical workstation (CH Instruments Co., USA). For impedance studies, the frequency range was between 0.1 Hz to 100 kHz with an AC signal of 7 mV amplitude. The applied bias voltage and AC amplitude were set at the V_{oc} of the DSSCs.

4. Results and Discussion:

4.1 Optical absorption and emission properties of ZnO and ZnO@PbS nanorods thin film:

Figure 1 shows the UV-Vis absorption spectra of ZnO nanorods (sample S1) and ZnO@PbS core-shell thin films (S2 to S4) with a different shell layer thickness. ZnO nanorods showed absorption edge at 368 nm, similar to reported in the literature [33]. The ZnO@PbS nanorods sample S2 showed absorption peaks at 372 and sample S3 showed peak at 428 nm respectively. The sample S4 showed two absorptions peaks; one at 379 nm and another at 514 nm. The absorption at 379 nm corresponds to ZnO and absorption at 514 nm corresponds to PbS nanostructure. The absorption of PbS layer at 514 nm was quite similar to the absorption of PbS quantum dot [29]. It has been observed that as the number of PbS layer on ZnO nanorod increased, the absorption of ZnO showed red shift, which might be due to the interaction between PbS layers and ZnO. For ZnO nanorods with 10 layers of PbS (sample S4) the absorption shifted smoothly to visible green region. There are three possible reasons for this visible absorption broadening of excitation bands: (a) increased inhomogeneous distribution of QDs sizes (b) strong QDs-QDs coupling and (c) strong QDs-ZnO interaction [34, 35]. This has been further discussed below in terms of the size quantum effect on the energy band alignment of PbS with respect to that of ZnO nanorods along with spatial separation of the electron and hole at the interface. Mostly, the change of the band gap of a nanoparticle is due to the increase or decrease of its bottom potential of the conduction band (CB) [36]. For bulk PbS, since its conduction band (CB) is lower in energy than the CB of ZnO, the electron transfer is impossible. The transfer of excited electrons from PbS layer into ZnO is due to the increase of CB of PbS caused by quantum size effect. Finally the photo generated electron gets transported to the external circuit through ZnO core nanorods, whereas holes with high oxidability accumulate in the valence band of PbS. Lower the PbS layer, higher will be its conduction band edge, leading to high driving force for injecting electrons into the

conduction band of ZnO nanorods. The band diagram of ZnO@PbS and the electron transfer mechanism under PbS layer excitation is shown in figure 2. Also, it is expected that the charge recombination will also be reduced by using ZnO nanorods as it can serve as privileged charge-transport pathways, the same phenomenon was observed in case of PbS/TiO_2 colloidal heterostructure [37].

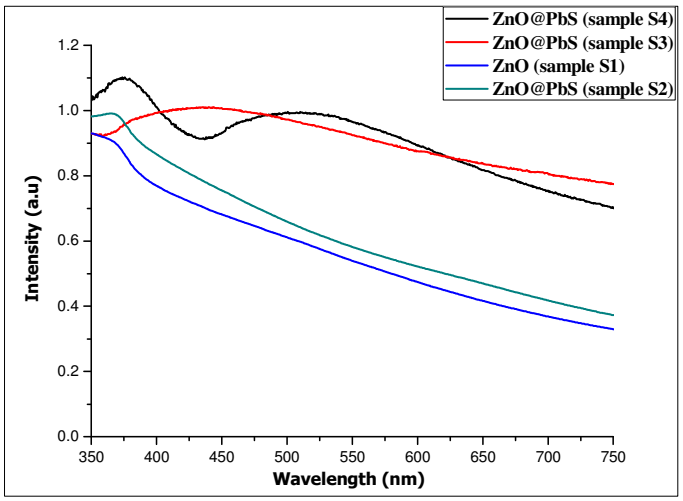

Figure 1. UV-Vis absorption spectra of ZnO nanorod and ZnO@PbS thin film (sample S1, S2, S3 and S4)

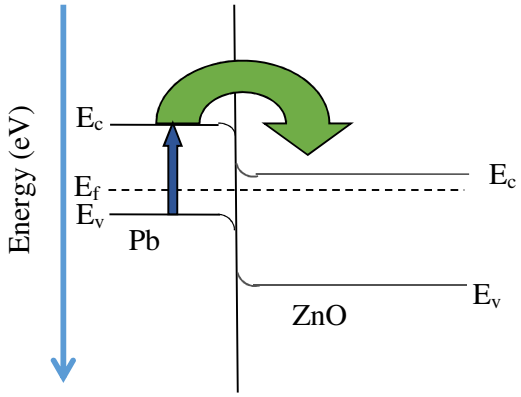

Figure 2. Energy band diagram of ZnO@PbS and electron transfer mechanism under PbS layer excitation

The photoluminescence (PL) spectrum is very sensitive to the electronic structure of the materials and is also very helpful to study the effect of successful growth of PbS on ZnO nanorods. In the present study, the photoluminescence spectra were measured at the

excitation wavelength of 350 nm at room temperature. For comparative study, the PL spectrum of samples S1 to S4 is given in the figure 3. The pure ZnO nanorods exhibited a narrow UV emission with its peaks at 360 nm and 378 nm [38, 39]. The UV emission peak is due to near band-edge transition. A blue emission band in the range of 380- 530 nm centered at 436 nm was observed in ZnO nanorods, which is associated with the recombination of carriers trapped at Z_{ni} (electrons) and V_{Zn} (holes) [40]. Although the ZnO@PbS nanorods showed similar UV emission bands as of ZnO, the band intensity is much weaker and blue emission bands almost disappeared. The UV emission intensity got reduced with increasing number of PbS layers. With the deposition of PbS layers, the structural characteristics of ZnO nanorods got changed. During PbS layer growth process, the S^{2-} anions present in the solution are easily captured by oxygen vacancies as oxygen and sulfur atoms have similar chemical properties [41]. The Pb^{2+} ions in solution occupy Zn vacancies. The Pb^{2+} and S^{2-} ions are captured by the surface defects of ZnO nanorods and provide the initial nucleation site for the surface growth of PbS layer, which reduces surface defects on ZnO nanorods. Therefore, the reduced photoluminescence intensity reasonably correlates with the reduced surface defects of ZnO nanorods.

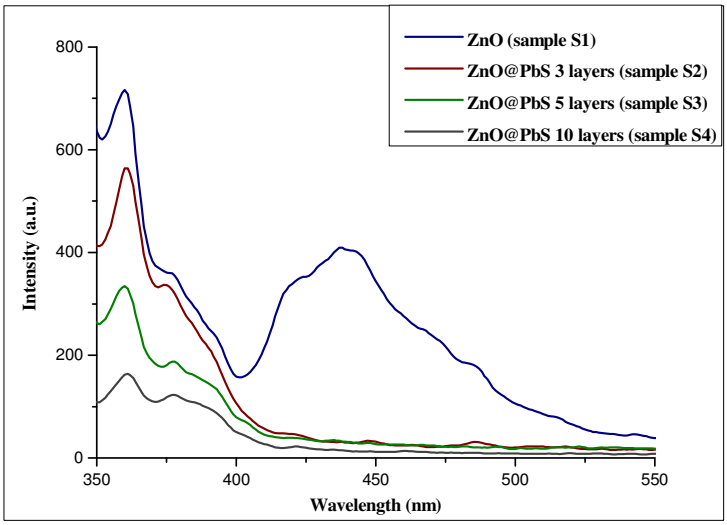

Figure 3 Photo luminescence spectra of ZnO (S1) and ZnO@PbS (S2 to S4) thin film

4.2 Growth Mechanism and surface morphology of ZnO@PbS core-shell thin film

In the base solution, Zn^{2+} ions can react with OH^- ions to form $Zn(OH)_2$, which then transformed into ZnO. As the concentration of free Zn^{2+} cations is sufficiently high the ZnO

nucleation start forming on the surface of ITO substrate. In the growth process of ZnO nanorods, the ZnO seed layer coated ITO substrate was dipped into the growth solution containing HMT and zinc nitrate. Where the HMT reacted with water and produced ammonia [42]. The ammonia tends to disintegrate water to produce OH^- anions in the solution. These generated OH^- anions react with Zn^{2+} to form Zn $(OH)_4^{2-}$ and finally ZnO nucleation is formed by the dehydration of intermediates. This homogeneous nucleation consumes ZnO precursors rapidly and causes early termination of growth of ZnO nanorods on the ITO substrate. In order to facilitate assembly of PbS layer on the ZnO nanorods surface, we used MPA linker to initiate a ligand exchange reaction. The molecular structure of MPA contains thiol (–SH) group on one end and carboxylic group (-COOH) on the other end. The carboxylic acid is attracted to the surface of the ZnO nanorods to form an ester linkage [43]. The thiol group of MPA is attracted to the PbS shell which forms a disulfide bond [44]. In DSSc, the linker molecules covalently attach the PbS to the ZnO surface without introducing a significant barrier for injection of the photo generated electron from the PbS to the ZnO nanorods. Growth mechanism of ZnO@PbS core-shell nanostructure thin film is pictorially depicted in figure 4. The FE-SEM image of ZnO seed layers, ZnO nanorods and ZnO@PbS thin film with 10 layers of PbS has been given in the figure 5 (a, b and c). The EDS of ZnO seed layer has been given in supportive information section. The uniform growth of ZnO nanorods has been confirmed from FESEM image. After PbS layers deposition on ZnO nanorods the surface of ZnO@PbS thin film become smooth. To study the size of ZnO nanorods and thickness of PbS layers has been confirm from TEM image. The length and width of ZnO nanorods (sample S1) was about 350- 450 nm and 60-70 nm, as shown in the figure 5 (d). The thickness of PbS was about 3-4 nm for ZnO@PbS nanorods (sample S4), as shown in the figure 5 (e). The selected-area electron-diffraction pattern (SAED) of the PbS shell is consistent with the cubic phase of PbS ring patterns showing (200) and (220) planes, as shown in the figure 5 (f). These patterns of SAED are composed of the regular clear diffraction dots, which indicate that the PbS shell is single crystalline.

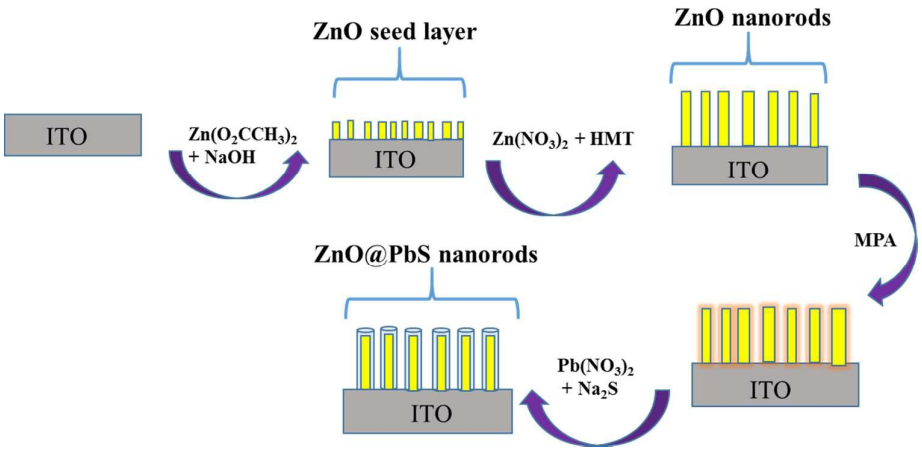

Figure 4 Schematic showing growth mechanism of ZnO@PbS core-shell nanostructure thin film

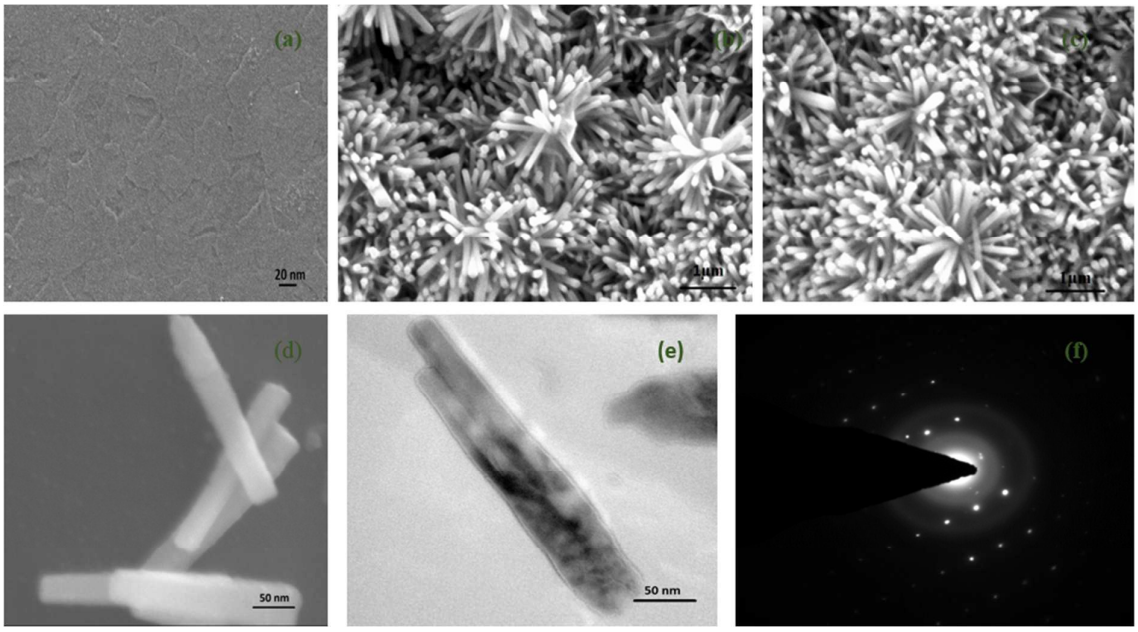

Figure 5 FE-SEM of ZnO seed layer (a), ZnO nanorods thin film (sample S1) (b) and ZnO@PbS nanorods thin film (sample S4) (c), TEM of ZnO nanorods (d) TEM of ZnO@PbS nanorods after 10 cycle of PbS (e) SAED pattern of PbS shell (f)

4.3 FTIR of ZnO@PbS nanorods:

The FTIR spectra of the neutral MPA ligand and as-synthesized ZnO@PbS nanorods are shown in the figure 6. The symmetric and asymmetric stretching vibrations of the carboxylate group of the charged MPA appear at 1418 and 1565 cm^{-1}, respectively. The absence of the S-

H stretching bond between 2633 cm^{-1} and 2561 cm^{-1} suggest the attachment of MPA molecule to PbS through chemical bond between thiols and dangling Zn atoms of the ZnO layer. The characteristic peaks at 2851 cm^{-1} and 2957 cm^{-1} attributed to C-H symmetric vibration almost disappeared after PbS coated to the surface of ZnO nanorod, similar result has been found in literature [45].

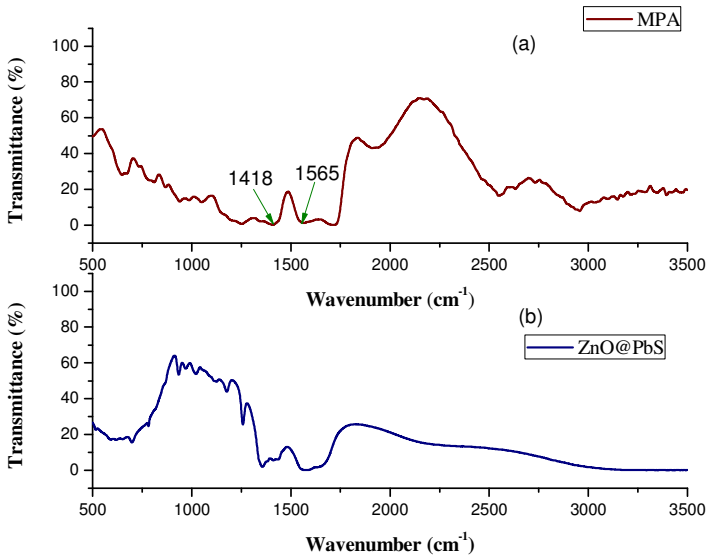

Figure 6 FTIR of (a) MPA (b) ZnO@PbS nanorods

4.4 Crystal Structure of ZnO nanorods and ZnO@PbS nanorods thin film

X-ray diffraction (XRD) was carried out to study the crystal structure of ZnO and ZnO@PbS nanostructure on ITO substrate. In sample S1, ZnO peaks have been identified at angles 34.35°, 36.29° (figure 7(a)), corresponding to {002} and {101} diffraction planes respectively, (JCPDS 36-1451, a = 0.325 nm, c = 0.521 nm). The XRD pattern contains the diffraction peaks of ITO substrate also at angles 31.64°, 35.19°, 50.63° and 60.01° corresponding to {222}, {400}, {440} and {622} planes (JCPDS 06-0416). This confirms the presence of well crystalline ZnO layer on ITO substrate. The {002} diffraction peak of ZnO nanorods is much stronger than XRD the previously reported samples. From the SEM of ZnO nanorods it is also observed that those are well aligned.

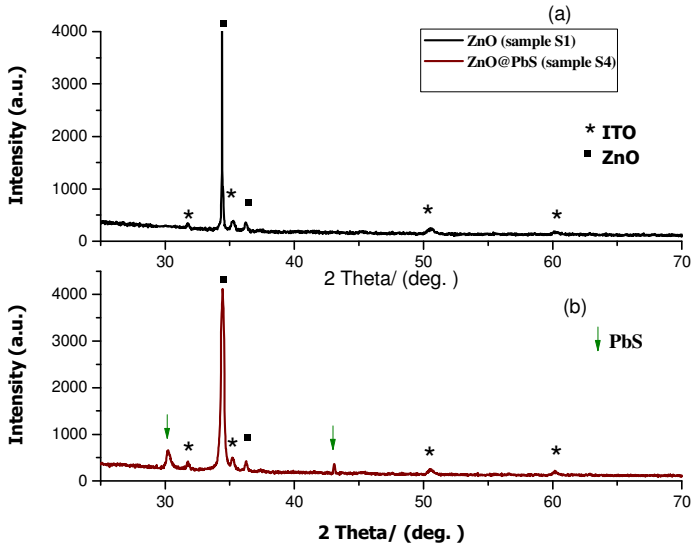

Figure 7 X-ray diffraction (XRD) patterns of ZnO nanorods (sample S1) (a) and core-shell ZnO@PbS (sample S4) (b) thin film

XRD pattern of ZnO@PbS shows the characteristic diffraction peaks of PbS at angle 30.1° and 43.06° corresponding to {200} and {220} planes, along with the peaks fo ZnO and ITO (figure 7(b)) [46]. The peaks corresponding to PbS confirms the presence of PbS. The d spacing of {200} and {220} PbS layer is 0.295 nm and 0.21 nm respectively. From these results, it can be inferred that there exists an occurrence of a separate process within the shell during the formation of PbS shell layer, adjacent to the ZnO nanorods. It appears that the ZnO@PbS nanostructures are well crystallized even though they were synthesized at a low temperature of 200 °C. The XRD result is consistent with the SAED pattern

4.5 Electrochemical impedance properties of thin films

The impedance is usually presented in the form of the Nyquist plot in which plots are between the real and imaginary. To obtain the better insight into dynamics of interfacial charge transfer process within the DSSCs, electrochemical impedance spectroscopy (EIS) was performed. In EIS, the impedance is usually presented in the form of Nyquist plot in which graph is plotted between the real and imaginary. The figure 8 shows the electrochemical impedance spectra recorded for ZnO@dye and ZnO@PbS@dye thin film based DSSCs. The equivalent circuit model of the impedance of different interfaces in DSSCs is presented in figure 9. The symbols have their usual meanings; R_s denotes solution resistance, R_1 stands for the charge transfer resistance of the ITO/ZnO or ITO/ZnO@PbS

interface and R_2 is the charge transfer resistance of ZnO/dye/electrolyte or ZnO@PbS/dye/electrolyte. The 'W' is finite Warburg impedance related element which is associated with diffusion processes and is influenced by the nature of electrode/electrolyte interface. The constant phase element (CPE) of the capacitance is related to a non-ideal frequency dependent capacitance due to a non-uniform distribution of current by the material heterogeneity. The resistances R_1 and R_2 directly influence the photovoltaic performance of the cell.

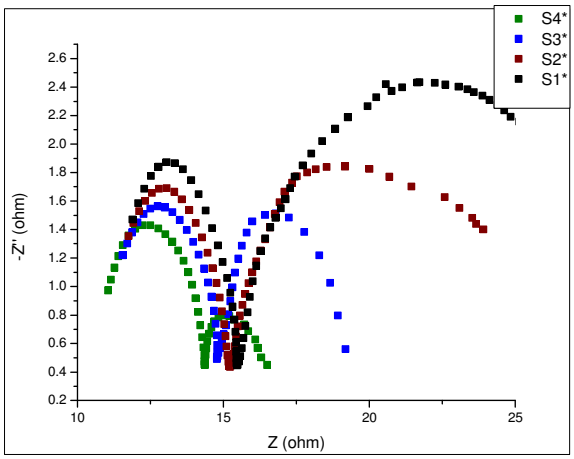

Figure 8 Impedance spectra of DSSCs at open-circuit conditions under illumination

The measured impedance spectra show two semicircles, one at very low frequency and other at medium and high frequency. In all four samples (S1* to S4*), the semicircle at the low frequency region is overlapped with the medium-frequency region. The Nyquist plot shows the overall charge transfer resistance for all samples. The results indicated that the performance improved with PbS layers on ZnO nanorods. These results reveal that the charge transfer resistance across ITO@ZnO of the S1* sample is high compared to the other three samples which may be due to high resistance at the interface of ITO substrate and ZnO nanorods. It may also delay the charge transfer at the ZnO@dye/electrolyte interface. The resistance R_1 of sample S1* may be the dominant factor responsible for the lower cell performance. Similarly, compared to sample S4*, the resistances R_1 and R_2 are higher for sample S1*, S2* and S3*. This result revealed that an electron can easily be transferred over the ZnO@PbS@dye surface, thereby enhancing the photocurrent generation and power efficiency of the solar cell.

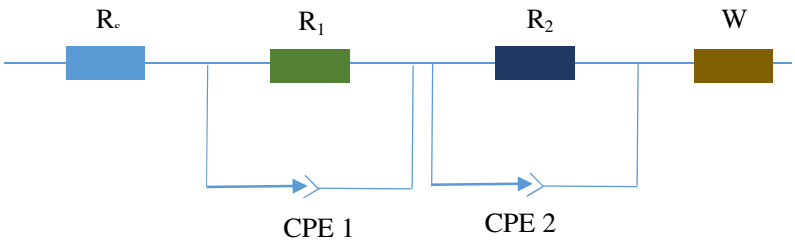

Figure 9. Electrochemical equivalent circuit

4.6 Photoconductivity behaviour of ZnO@Dye and ZnO@PbS@Dye thin film:

To study the effect of the PbS layer thickness of ZnO thin film, we investigated the responses of the transient photocurrent of samples S1* to S4* under visible light irradiation. It has been observed that the ZnO@dye (sample S1*) thin film exhibited lower photoelectric current because ZnO has visible blindness. The photo current was generated only from N719 dye. Whereas in ZnO@PbS@Dye thin film, the photoelectric current depends upon the number of PbS layers on ZnO thin film as shown in the figure 10. The photocurrent values reached 1.67, 4.36, 7.84 and 8.42 mA in 70 sec for sample S2*, S3* and S4* respectively. These results also strongly indicate that the photocurrent enhancement is mainly due to photo generated electrons from PbS layers and prolonged effect in ZnO@PbS samples. Furthermore, it is suggested that the ZnO@PbS@dye thin film has a great potential application as a visible-light photocatalyst material.

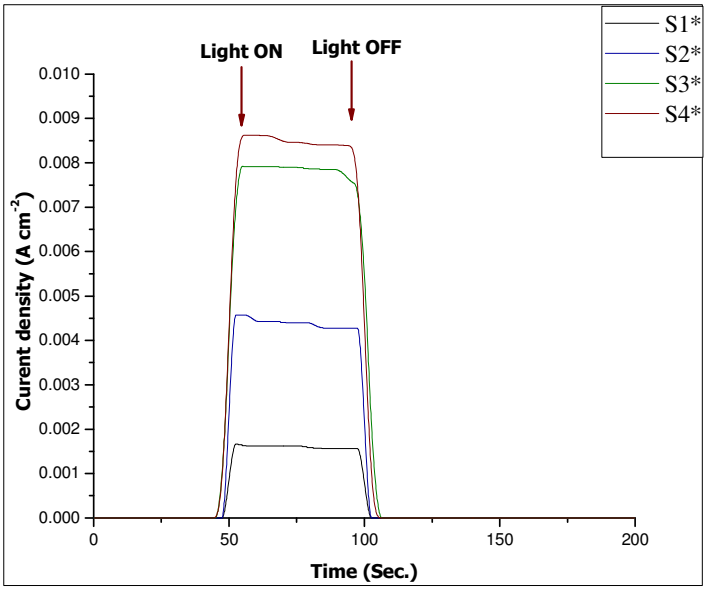

Figure 10 Transient photo current response of ZnO@Dye and ZnO@PbS@Dye thin film with different PbS shell layers under zero bias voltage

4.7 Photocurrent-voltage studies:

The J-V measurements were carried out for DSSc with ZnO@Dye (sample S1*) and ZnO@PbS@Dye (sample S2* to S4*) thin film photo electrodes, under same environmental condition. The J-V measurements of ZnO@PbS thin film based solar cell were made in redox liquid electrolyte consisting of 1 M Na_2S and 1 M S in aqueous solution. The effect of PbS layers thickness on performance of solar cell has been given in supporting information section. The photoelectrodes were assembled with platinized ITO glass counter electrodes and liquid electrolyte. The photovoltaic performance obtained for different PbS layer thickness is summarized in figure 11. These solar cell parameter were calculated by equations bellow [47].

$$FF = \frac{P_{max}}{I_{SC}\,V_{OC}} = \frac{I_{max}V_{max}}{I_{SC}\,V_{OC}} \qquad (2)$$

$$\eta = \frac{P_{max}}{P_{in}} = \frac{I_{SC}V_{OC}FF}{P_{in}} \qquad (3)$$

$$P_{max} = I_{sc}V_{oc} \qquad (4)$$

It has been found that the open circuit voltage (V_{oc}) and the short circuit current (J_{sc}) increased gradually with an increase in the number of PbS layers. The fill factor (FF) was maximum for thin film with 10 PbS layers. Thus, adjusting the thickness of PbS shell layers, seems to be an effective approach to improve overall photovoltaic performance of DSSc solar cell. The maximum energy conversion efficiency and fill factor was 6.59% and 0.75 respectively for ZnO@PbS core-shell nanorods with 10 layers of PbS. As the dye layer coating is uniform for the entire samples, the different PbS layers thickness was only responsible for the enhancement of open circuit voltage and overall performance of solar cell. All device performance parameters are listed in table 1.

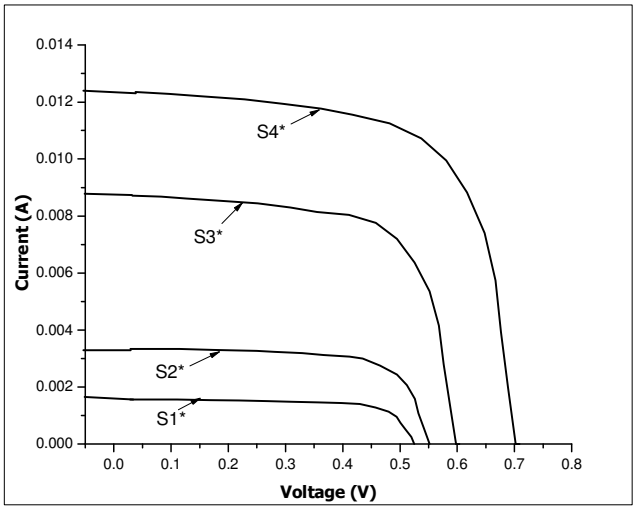

Figure 11 Photocurrent - voltage response of the DSSC cell with ZnO@Dye and ZnO@PbS@Dye nanostructure thin film

Sample Name	V_{oc} (V)	J_{sc} (mA)	FF	Efficiency (η)
S1*	0.53	1.63	0.76	0.65
S2*	0.56	3.31	0.73	1.35
S3*	0.64	8.77	0.72	4.04
S4*	0.71	12.39	0.75	6.59

Table 1 Averaged Photovoltaic Parameters of DSSc based on four samples

4.8 Charge transfer mechanism in ZnO@PnS@Dye thin film

The resulting solar cell consisted of a ZnO nanorods thin film electrode and layers of PbS as the sensitizer. The ZnO nanorods served as both as a stabilizer for the PbS layers and a substrate for the second absorber, a N719 dye layer. For an efficient operation of the ZnO@PbS thin film based DSSc, we require a high yield of interfacial charge separation and the minimization of recombination losses between the photo injected electrons in the ZnO and the PbS layer. Figure 12 represents the scheme of energy diagram for the formation of a cascade energy band matching by introducing the PbS layer between the ZnO and dye N719. The energy levels of ZnO, PbS and the N719 dye are taken from the literature [48]. The conduction band of PbS nanostructure is in between the excited state of N719 dye and the conduction band of ZnO. During the charge transfer process, the photo generated electron jumps from the LUMO of the dye to the conduction band (E_c) of PbS layer, and from the E_c of PbS layer to the Ec of ZnO as the work function of ZnO (-5.2 eV) is higher than the PbS (-4.5 eV).

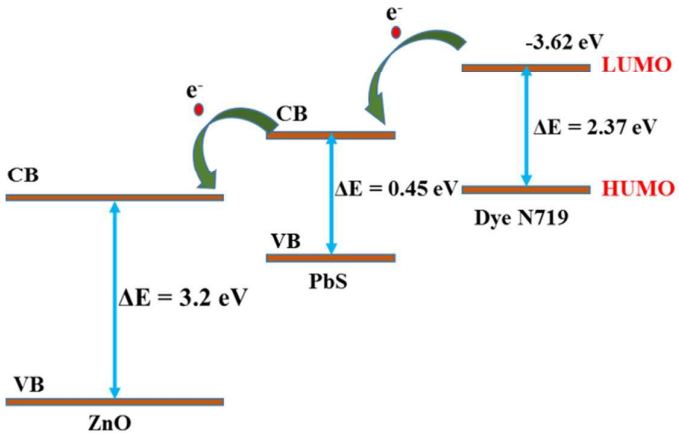

Figure 12 Scheme of energy diagram for formation of cascade energy band matching by introducing the PbS layer between the ZnO and dye N719

5. Conclusion:

In summary, the novel ZnO@PbS thin film has been fabricated using a simple SILER method, providing remarkable performance. The PbS coating on ZnO nanorods show that the absorption of ZnO@PbS shifted smoothly from UV to visible region. PbS layers supresses the surface defect of ZnO nanorods and enhance the charge separation process at the interface of ZnO and PbS layer. The PbS layers improve the photovoltaic and photoconductive performance of ZnO@PbS nanorods based thin film.

Acknowledgements:

The authors acknowledge CSIR for research fellowships and supports extended for this work.

Reference:

1. V. P. S. Perera, P. K. D. D. P. Pitigala, P. V. V. Jayaweera, K. M. P. Bandaranayake and K. Tennakone, *The Journal of Physical Chemistry B*, 2003, 107, 13758-13761.
2. T. Prakash, *Electron. Mater. Lett.*, 2012, 8, 231-243.
3. A. Kongkanand, K. Tvrdy, K. Takechi, M. Kuno and P. V. Kamat, *Journal of the American Chemical Society*, 2008, 130, 4007-4015.
4. C.-H. Chang, T.-K. Huang, Y.-T. Lin, Y.-Y. Lin, C.-W. Chen, T.-H. Chu and W.-F. Su, *Journal of Materials Chemistry*, 2008, 18, 2201-2207.
5. K. Yu and J. Chen, *Nanoscale Research Letters*, 2009, 4, 1-10.
6. M. Seol, H. Kim, Y. Tak and K. Yong, *Chemical Communications*, 2010, 46, 5521-5523.
7. I. Moreels, K. Lambert, D. Smeets, D. De Muynck, T. Nollet, J. C. Martins, F. Vanhaecke, A. Vantomme, C. Delerue, G. Allan and Z. Hens, *ACS Nano*, 2009, 3, 3023-3030.
8. M. Nam, J. Park, S.-W. Kim and K. Lee, *Journal of Materials Chemistry A*, 2014, 2, 3978-3985.
9. S. B. Ambade, R. S. Mane, A. V. Ghule, G.-W. Lee, R. Sharma, O.-s. Joo, R. B. Ambade, S.-H. Lee and S.-H. Han, *Journal of Photochemistry and Photobiology A: Chemistry*, 2011, 217, 267-270.
10. P. Maity, T. Debnath and H. N. Ghosh, *The Journal of Physical Chemistry Letters*, 2013, 4, 4020-4025.
11. C. Li, L. Yang, J. Xiao, Y.-C. Wu, M. Sondergaard, Y. Luo, D. Li, Q. Meng and B. B. Iversen, *Physical Chemistry Chemical Physics*, 2013, 15, 8710-8715.
12. J. H. Bang and P. V. Kamat, *ACS Nano*, 2011, 5, 9421-9427.
13. V. Sholin, A. J. Breeze, I. E. Anderson, Y. Sahoo, D. Reddy and S. A. Carter, *Solar Energy Materials and Solar Cells*, 2008, 92, 1706-1711.
14. M. A. Hines and G. D. Scholes, *Advanced Materials*, 2003, 15, 1844-1849.
15. L. Bakueva, S. Musikhin, M. A. Hines, T.-W. F. Chang, M. Tzolov, G. D. Scholes and E. H. Sargent, *Applied Physics Letters*, 2003, 82, 2895-2897.
16. A. Kar and A. Patra, *Journal of Materials Chemistry C*, 2014, 2, 6706-6722.
17. H. Wang, T. Kubo, J. Nakazaki, T. Kinoshita and H. Segawa, *The Journal of Physical Chemistry Letters*, 2013, 4, 2455-2460.
18. J. Gao, J. M. Luther, O. E. Semonin, R. J. Ellingson, A. J. Nozik and M. C. Beard, *Nano Letters*, 2011, 11, 1002-1008.
19. P. R. Brown, R. R. Lunt, N. Zhao, T. P. Osedach, D. D. Wanger, L.-Y. Chang, M. G. Bawendi and V. Bulović, *Nano Letters*, 2011, 11, 2955-2961.
20. S. M. Willis, C. Cheng, H. E. Assender and A. A. R. Watt, *Nano Letters*, 2012, 12, 1522-1526.
21. J. Jean, S. Chang, P. R. Brown, J. J. Cheng, P. H. Rekemeyer, M. G. Bawendi, S. Gradečak and V. Bulović, *Advanced Materials*, 2013, 25, 2790-2796.
22. X. Song, M. Wang, J. Deng, Y. Ju, T. Xing, J. Ding, Z. Yang and J. Shao, *Journal of Power Sources*, 2014, 269, 661-670.
23. S. B. Bubenhofer, C. M. Schumacher, F. M. Koehler, N. A. Luechinger, R. N. Grass and W. J. Stark, *The Journal of Physical Chemistry C*, 2012, 116, 16264-16270.
24. A. N. Jumabekov, F. Deschler, D. Böhm, L. M. Peter, J. Feldmann and T. Bein, *The Journal of Physical Chemistry C*, 2014, 118, 5142-5149.
25. D. Wang, H. Zhao, N. Wu, M. A. El Khakani and D. Ma, *The Journal of Physical Chemistry Letters*, 2010, 1, 1030-1035.
26. I. J. Kramer, L. Levina, R. Debnath, D. Zhitomirsky and E. H. Sargent, *Nano Letters*, 2011, 11, 3701-3706.

27. G. I. Koleilat, X. Wang, A. J. Labelle, A. H. Ip, G. H. Carey, A. Fischer, L. Levina, L. Brzozowski and E. H. Sargent, *Nano Letters*, 2011, 11, 5173-5178.
28. Y. Yang, W. Rodríguez-Córdoba, X. Xiang and T. Lian, *Nano Letters*, 2011, 12, 303-309.
29. C. Ratanatawanate, C. Xiong and K. J. Balkus, *ACS Nano*, 2008, 2, 1682-1688.
30. L. Etgar, T. Moehl, S. Gabriel, S. G. Hickey, A. Eychmüller and M. Grätzel, *ACS Nano*, 2012, 6, 3092-3099.
31. F. Boon, D. Moerman, D. Laurencin, S. Richeter, Y. Guari, A. Mehdi, P. Dubois, R. Lazzaroni and S. Clément, *Langmuir*, 2014, DOI: 10.1021/la502944g.
32. M. Misra, P. Kapur, C. Ghanshyam and M. Singla, *J Mater Sci: Mater Electron*, 2013, 24, 3800-3804.
33. A. R. Marlinda, N. M. Huang, M. R. Muhamad, M. N. An'amt, B. Y. S. Chang, N. Yusoff, I. Harrison, H. N. Lim, C. H. Chia and S. V. Kumar, *Materials Letters*, 2012, 80, 9-12.
34. R. Ihly, J. Tolentino, Y. Liu, M. Gibbs and M. Law, *ACS Nano*, 2011, 5, 8175-8186.
35. J. Tang, L. Brzozowski, D. A. R. Barkhouse, X. Wang, R. Debnath, R. Wolowiec, E. Palmiano, L. Levina, A. G. Pattantyus-Abraham, D. Jamakosmanovic and E. H. Sargent, *ACS Nano*, 2010, 4, 869-878.
36. P. V. Kamat, *The Journal of Physical Chemistry C*, 2008, 112, 18737-18753.
37. K. P. Acharya, N. N. Hewa-Kasakarage, T. R. Alabi, I. Nemitz, E. Khon, B. Ullrich, P. Anzenbacher and M. Zamkov, *The Journal of Physical Chemistry C*, 2010, 114, 12496-12504.
38. A. Layek, S. De, R. Thorat and A. Chowdhury, *The Journal of Physical Chemistry Letters*, 2011, 2, 1241-1247.
39. H. Zhang, L. Shen and S. Guo, *The Journal of Physical Chemistry C*, 2007, 111, 12939-12943.
40. M. Norek, G. Łuka, M. Godlewski, T. Płociński, M. Michalska-Domańska and W. Stępniowski, *Appl Phys A*, 2013, 111, 265-271.
41. T. Gao, Q. Li and T. Wang, *Chemistry of Materials*, 2005, 17, 887-892.
42. H. Singh, S. Bhagwat, S. Jouen, B. Lefez, A. A. Athawale, B. Hannoyer and S. Ogale, *Physical Chemistry Chemical Physics*, 2010, 12, 3246-3253.
43. J. W. Spalenka, P. Gopalan, H. E. Katz and P. G. Evans, *Applied Physics Letters*, 2013, 102, -.
44. L. Etgar, J. Park, C. Barolo, M. K. Nazeeruddin, G. Viscardi and M. Graetzel, *ACS Applied Materials & Interfaces*, 2011, 3, 3264-3267.
45. A. Aboulaich, M. Geszke, L. Balan, J. Ghanbaja, G. Medjahdi and R. Schneider, *Inorganic Chemistry*, 2010, 49, 10940-10948.
46. D. Buso, P. Falcaro, S. Costacurta, M. Guglielmi, A. Martucci, P. Innocenzi, L. Malfatti, V. Bello, G. Mattei, C. Sada, H. Amenitsch, I. Gerdova and A. Haché, *Chemistry of Materials*, 2005, 17, 4965-4970.
47. S. Sönmezoğlu, R. Taş, S. Akın and M. Can, *Applied Physics Letters*, 2012, 101, -.
48. K. P. Bhandari, P. J. Roland, H. Mahabaduge, N. O. Haugen, C. R. Grice, S. Jeong, T. Dykstra, J. Gao and R. J. Ellingson, *Solar Energy Materials and Solar Cells*, 2013, 117, 476-482.

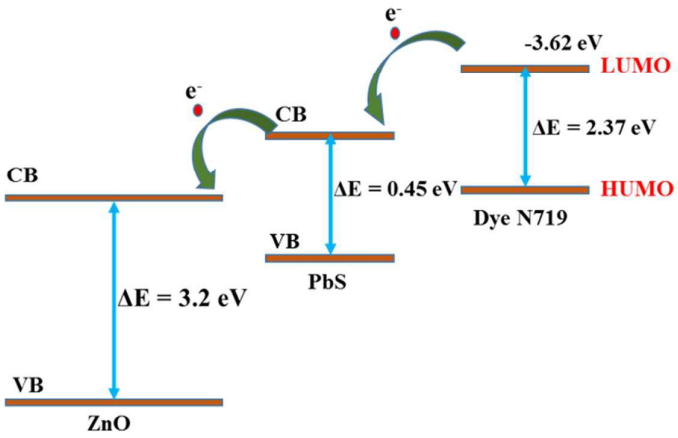

Scheme of energy diagram for formation of cascade energy band matching by introducing the PbS layer between the ZnO and dye N719